# Doppler optical coherence tomography with a micro-electro-mechanical membrane mirror for high-speed dynamic focus tracking

**Victor X. D. Yang, Youxin Mao, Beau A. Standish, Nigel R. Munce, Stephanie Chiu, Daina Burnes, Brian C. Wilson, and I. Alex Vitkin**

*Ontario Cancer Institute, University Health Network, Toronto, Ontario, Canada*

**Phillip A. Himmer and David L. Dickensheets**

*Department of Electrical and Computer Engineering, Montana State University, Bozeman, Montana 59717*

Received October 17, 2005; revised January 15, 2006; accepted February 2, 2006; posted February 8, 2006 (Doc. ID 65435)

An elliptical microelectromechanical system (MEMS) membrane mirror is electrostatically actuated to dynamically adjust the optical beam focus and track the axial scanning of the coherence gate in a Doppler optical coherence tomography (DOCT) system at 8 kHz. The MEMS mirror is designed to maintain a constant numerical aperture of ~0.13 and a spot size of ~6.7 $\mu$m over an imaging depth of 1 mm in water, which improves imaging performance in resolving microspheres in gel samples and Doppler shift estimation precision in a flow phantom. The mirror's small size (1.4 mm × 1 mm) will allow integration with endoscopic MEMS-DOCT for *in vivo* applications. © 2006 Optical Society of America

*OCIS codes:* 170.4500, 170.3880, 170.3340, 170.4580, 170.3890, 170.7050.

Wide-bandwidth light sources have allowed submicrometer axial resolution in optical coherence tomography (OCT),[1] but improvement of lateral resolution is hindered by the trade-off between numerical aperture (NA) and depth of focus, especially for endoscopic applications. Bulk optics focus tracking,[2] fusion of multiple images acquired at different focal depths,[1] a multichannel OCT fiber array,[3] lateral priority OCT,[4] and a liquid-filled polymer lens[5] have been reported as means to address this issue. These methods have yet to be tested with Doppler OCT systems. We previously reported the concept of a microelectromechanical system (MEMS) membrane mirror for dynamic focus tracking in a preliminary paper.[6] In this Letter we report enhanced OCT signal intensity and Doppler shift measurement precision using such a tracking system with improved optical design.

An elliptical MEMS membrane mirror was incorporated into the sample arm of a high axial scan rate (8 kHz sinusoidally) Doppler optical coherence tomography (DOCT) system with center wavelength $\lambda_0 = 1.3$ $\mu$m (details provided in Ref. 7) for dynamic focus tracking, as shown in Fig. 1. The DOCT images were acquired at 1 frame/s with 8000 axial scans per image and 512 samples per axial scan. The elliptical mirror[8,9] was fabricated using a modified surface micromachining process on a silicon (100) wafer, resulting in a 1 $\mu$m thick low residual stress (~50 MPa) silicon nitride membrane suspended over the silicon substrate with a 13 $\mu$m air gap. A sputtered 100 nm thick gold layer can deflect the membrane electrostatically and provide near 100% optical reflectivity in the near-IR spectrum. The major and minor axes of the elliptical mirror were 1.41 and 1 mm, respectively, suitable for a $D = 1$ mm diameter beam incident at 45°. Figure 1(b) shows an interferometric ring pattern of the curved membrane mirror surface with voltage applied to deflect the mirror. The central deflection of the membrane, $\delta$, is proportional to the square of the applied voltage, with $\delta_{max} = 4.7$ $\mu$m at 173 V. Figure 1(c) shows the details of the MEMS scan tip of the DOCT system, where the membrane mirror is positioned in the collimated beam path at one focal length from the objective lens (aspherical lens, $f = 3.9$ mm, NA = 0.128). The corresponding $1/e^2$

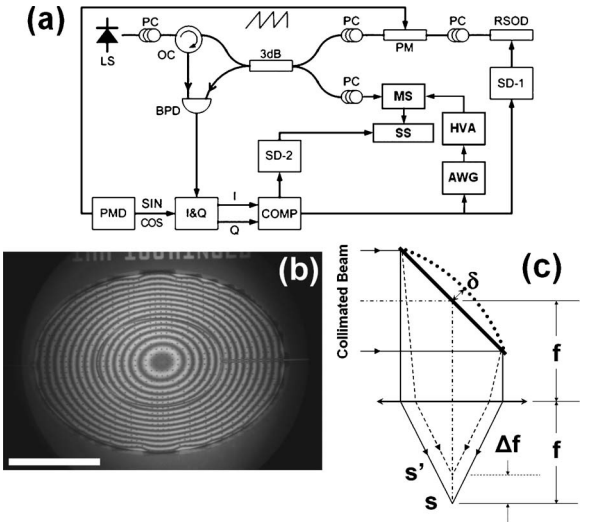


Fig. 1. (a) Schematic of the MEMS-DOCT system: LS, broadband light source; PC, polarization controller; OC, optical circulator; BPD, balanced photodetector; PM, phase modulator; PMD phase modulator driver; I&Q, in-phase and quadrature demodulator; RSOD, rapid scanning optical delay; SD-1, SD-2, depth and transverse scan drivers, respectively; MS, MEMS scan tip; SS, sample stage; HVA, high-voltage amplifier; AWG, arbitrary waveform generator; COMP, computer. (b) Interferometric image of an elliptical MEMS membrane mirror with a central deflection of ~4.7 $\mu$m, with small curvature aberrations near the edge. Bar = 500 $\mu$m. (c) Schematic of the MEMS scan tip optics. MEMS-off focus, S; MEMS-on focus, S′.

 

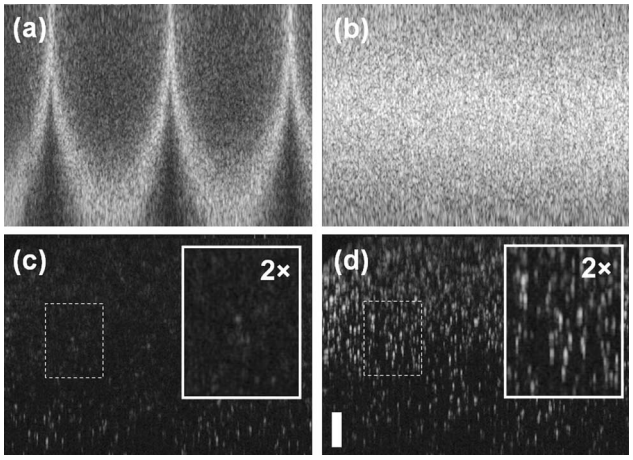


Fig. 2. (a) Intensity OCT image of a 0.5% Intralipid suspension obtained while the MEMS membrane was driven by a 0.75 Hz, unsynchronized triangular waveform, showing the sweeping pattern of the focal zone. (b) MEMS-OCT imaging when the focus was tracking the axial scan, showing overall increased signal intensity along the depth. (c) MEMS-off and (d) MEMS-on images of a sparse gel of 4.5 $\mu$m microsphere suspension, with the insets showing magnified regions in the dashed boxes. Bar = 100 $\mu$m.

spot size is 6.7 $\mu$m, and the depth of field, $2z_0 = 2\lambda_0 n/\pi \mathrm{NA}^2$, is 67 $\mu$m ($n = 1.33$), outside of which the lateral resolution worsens rapidly. It can be shown that deflecting the center of the membrane by $\delta$ will move the mirror's focus from $S$ to $S'$, resulting in a change of focus, $\Delta f = 4n\delta/\sqrt{2}\mathrm{NA}^2$, without affecting the NA. Simulation of the system [shown schematically in Fig. 1(c)] with ZEMAX software demonstrates a diffraction-limited system with less than 1% variation in spot size through the full range (~1 mm in water) of focus tracking when the membrane is deflected from rest to approximately 4.3 $\mu$m and the wavefront peak–valley variation is less than $\lambda_0/10$, where most of the aberration is contributed by the objective lens.

To experimentally examine the performance of this scheme, we first verified the motion of the focal zone while imaging a 0.5% Intralipid suspension. Figure 2(a) shows the focal zone changing parabolically, as expected from a triangular waveform actuating voltage with an amplitude of 165 V. Driving the membrane with a bipolar sinusoidal waveform at half the frequency of the rapid scanning optical delay will allow approximate tracking of the focal zone with the axial scan. Figure 2(b) shows the effect of using an external clock to phase lock the driving waveforms and the rapid scanning optical delay, demonstrating enhanced OCT signal intensity along the entire depth of scanning. The relative reduction of signal intensity at the top and bottom of the image was likely due to mismatch between the focal zone and the coherence gate towards the ends of the tracking range.

The improvement in image quality by focus tracking could be further seen in Figs. 2(c) and 2(d), where a sparse ($1.3 \times 10^8$ spheres/mm$^{-3}$) solution of 4.5 $\mu$m microspheres embedded in gel was used as a resolution target. When the MEMS mirror tracking was turned off, the OCT system showed identifiable microspheres in the focal plane at the bottom of the image. After focus tracking was turned on, the blurring above the static focal plane was significantly reduced, along with increased signal intensity, which allowed visualization of the microspheres throughout the image. Both images were obtained at the same location in the gel sample. The inhomogeneous distribution of the microspheres was due to density differences between the gel and the spheres.

Since the precision of the Doppler shift estimation improves as the signal-to-noise ratio increases,[7,10] we also expect an enhancement in Doppler flow imaging specifically in terms of reduction of the velocity variance. This is demonstrated in Fig. 3 by a flow phantom of 0.5% Intralipid solution driven by an IV pump at 5.5 $\mu$L/s. The lumen diameter was 600 $\mu$m, and the peak flow velocity at the center of the lumen was approximately 39 mm/s, assuming a parabolic flow profile (Doppler angle ~88°). As shown in Fig. 3(a), when the MEMS mirror tracking was turned off, the focal zone was positioned at the bottom of the image. The vertical streaks were inhomogeneities due to changes in the concentration of Intralipid flowing through the imaging plane during lateral scanning. When the focal zone was moved through the different depths as shown in Fig. 3(b), a corresponding region of low-velocity variance could be observed, interspersed with high-variance regions consistent with "chaotic" color Doppler pixels showing a large spread of the Doppler shift estimates. The reduction in velocity variance could be observed throughout the image when the MEMS tracking was turned on, as shown in Fig. 3(c).

To demonstrate quantitatively the improved precision of Doppler shift estimation, $M$-mode (axial Doppler shift versus time at a fixed lateral location) DOCT images were obtained while the MEMS track-

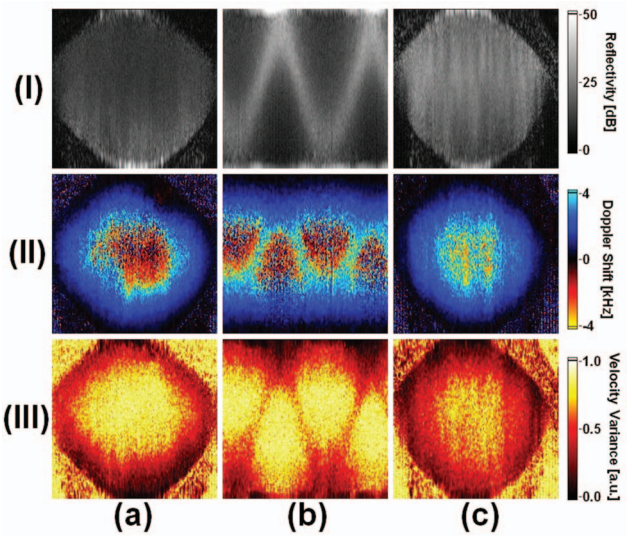


Fig. 3. MEMS-DOCT imaging of a flow phantom using Intralipid solution pumped through a 600 $\mu$m diameter tube. Rows I, II, and III: intensity, Doppler shift, and velocity variance images, respectively. Column (a) MEMS off; (b) $M$-mode imaging with the MEMS membrane driven by a 1.2 Hz, unsynchronized sinusoidal waveform; (c) MEMS membrane driven to track the axial scan.

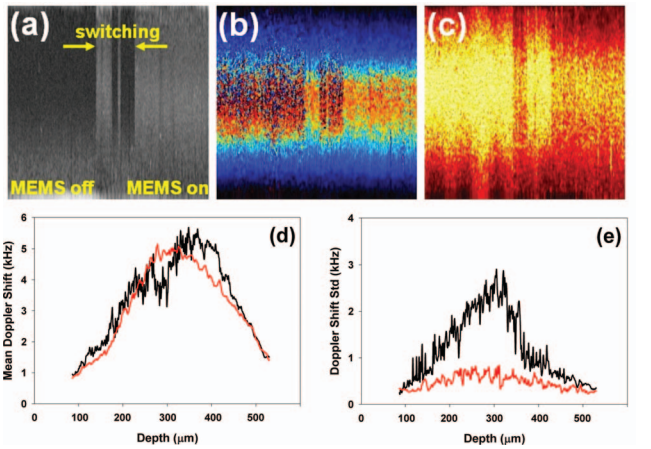


Fig. 4. $M$-mode DOCT images of the 600 $\mu$m diameter flow phantom with MEMS tracking turned on at the middle of the images (a) Intensity, (b) Doppler shift, and (c) velocity variance images [scales are identical to Fig. 3(b)]. (d) and (e) show the representative mean and standard deviation of the Doppler shift estimates in the flow phantom under MEMS-off (black) and MEMS-on (red) conditions, respectively. Each curve shows the statistics from 50 axial scans. The peak Doppler shift after phase unwrapping agrees with the experimental condition.

ing system was operating, as shown in Fig. 4. Besides the signal intensity enhancement, the Doppler shift estimation showed less velocity variance with the MEMS tracking turned on. As shown in Figs. 4(d) and 4(e), MEMS tracking provided approximately four times better precision of the Doppler frequency shift estimation at the center of the flow phantom.

Incorporating moving components into the DOCT interferometer typically carries the risk of introducing vibrational noises and degradation of performance. We have demonstrated that careful synchronization between the MEMS membrane mirror (with a peak velocity of $\sim$69 mm/s at the center of the membrane) and the DOCT scanning system could result in enhanced signal intensity and Doppler shift estimate precision without deleterious effects. A good figure of merit ($M$) of the MEMS tracking system is the number of focal zones swept through the axial scan, $M=\Delta f/2z_0=2\pi\delta/\sqrt{2}\lambda_0$, which is $\sim$14 for our current system and can be increased by larger membrane deflection with improved fabrication processes. The membrane mirror is best suited for continuous focus tracking in time-domain OCT systems and can be operated in discrete steps to form multiple focal zones in frequency-domain OCT systems with a trade-off in imaging speed.[11] This trade-off may be alleviated by the recent advances in k-space resampling.[12] We also note that optimal tracking performance depends on the tissue surface topology (determination of which may require an axial prescan) and the refractive-index profile in tissue (which may be approximated from *a priori* measurements for layered structures). A different driving waveform for each individual axial scan can be generated for optimal performance. Alternatively, an adaptive feedback control process can be employed to maximize the local OCT signal intensity during scanning, given that the wide-frequency response (>40 kHz) of the MEMS membrane mirrors will support fast feedback-loop reactions. Since the Doppler shift estimation precision is influenced by beam NA and diameter,[13,14] the constant lateral resolution and NA accompanying the coherence gate axial scan may offer enhanced performance of tissue microcirculation imaging for endoscopic optical coherence microscopy devices.

This work was supported by the Canadian Institutes of Health Research, Photonics Research Ontario, NASA, and the National Science Foundation. V. X. D. Yang's e-mail address is victor.yang@utoronto.ca.

## References

1. W. Drexler, U. Morgner, F. X. Kärtner, C. Pitris, S. A. Boppart, X. D. Li, E. P. Ippen, and J. G. Fujimoto, Opt. Lett. **24**, 1221 (1999).
2. J. M. Schmitt, S. L. Lee, and K. M. Yung, Opt. Commun. **142**, 203 (1997).
3. V. X. D. Yang, N. Munce, J. Pekar, M. L. Gordon, S. Lo, N. E. Marcon, B. C. Wilson, and I. A. Vitkin, Opt. Lett. **29**, 1754 (2004).
4. M. J. Cobb, X. Liu, and X. D. Li, Opt. Lett. **30**, 1680 (2005).
5. A. Divetia, T. H. Hsieh, J. Zhang, Z. Chen, M. Bachman, and G. P. Li, Appl. Phys. Lett. **86**, 103902 (2005).
6. B. Qi, P. A. Himmer, M. L. Gordon, V. X. D. Yang, D. L. Dickensheets, and I. A. Vitkin, Opt. Commun. **232**, 123 (2004).
7. V. X. D. Yang, M. L. Gordon, B. Qi, J. Pekar, S. Lo, E. Seng-Yue, A. Mok, B. C. Wilson, and I. A. Vitkin, Opt. Express **11**, 794 (2003).
8. P. A. Himmer, D. L. Dickensheets, and R. A. Friholm, Opt. Lett. **26**, 1280 (2001).
9. P. A. Himmer and D. L. Dickensheets, in Proc. SPIE **4983**, 296 (2003).
10. S. Yazdanfar, C. Yang, M. V. Sarunic, and J. A. Izatt, Opt. Express **13**, 410 (2005).
11. R. Huber, M. Wojtkowski, J. G. Fujimoto, J. Y. Jiang, and A. E. Cable, Opt. Express **13**, 10523 (2005).
12. T. S. Ralston, D. L. Marks, P. S. Carney, and S. A. Boppart, in Proc. SPIE **6079**, 312 (2006).
13. Y. Zhao, Z. Chen, C. Saxer, Q. Shen, S. Xiang, J. F. de Boer, and J. S. Nelson, Opt. Lett. **25**, 1358 (2000).
14. S. G. Proskurin, Y. He, and R. K. Wang, Opt. Lett. **28**, 1227 (2003).